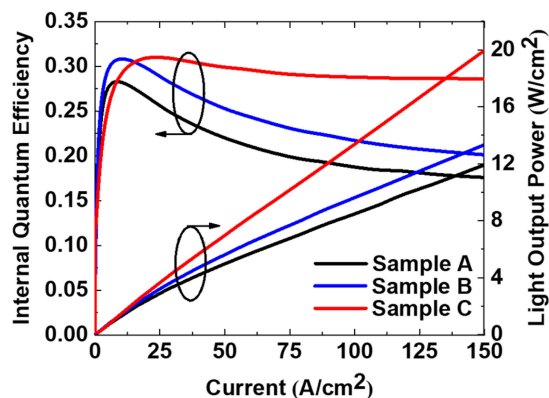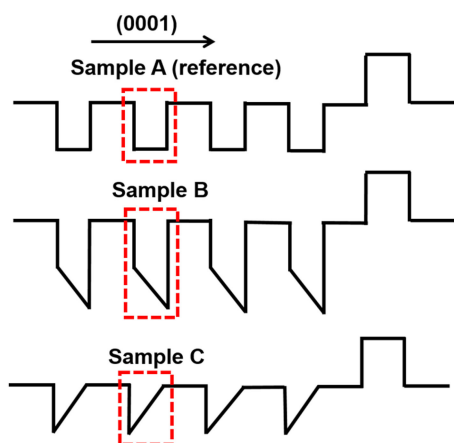# Enhanced Performance of an AlGaN-Based Deep-Ultraviolet LED Having Graded Quantum Well Structure

Huabin Yu
Qian Chen
Zhongjie Ren
Meng Tian
Shibing Long
Jiangnan Dai
Changqing Chen
Haiding Sun

Enhanced Performance of an AlGaN-Based Deep-Ultraviolet LED Having Graded Quantum Well Structure

Huabin Yu,[1] **Qian Chen,**[2] **Zhongjie Ren** ⊙**,**[3] **Meng Tian,**[1]
Shibing Long ⊙**,**[1] **Jiangnan Dai,**[2] **Changqing Chen** ⊙**,**[2]
and Haiding Sun ⊙ [1]

[1]School of Microelectronics, University of Science and Technology of China, Hefei 230026, China
[2]Wuhan National Laboratory for Optoelectronics, Huazhong University of Science and Technology, Wuhan 430074, China
[3]Jacobs School of Engineering, University of California San Diego, La Jolla, CA 92093 USA

Abstract: AlGaN-based deep ultraviolet light-emitting diodes (DUV LEDs) suffer from severe quantum confined Stark effect (QCSE) due to the strong polarization field in the quantum wells (QWs) grown on *c*-plane substrates. In this paper, we propose a novel DUV LED structure embedded with graded QWs in which the Al composition was linearly changed to screen the QCSE. A significant increase of the internal quantum efficiency and thus an enhancement of the light output power by nearly 67% can be achieved, attributing to the improvement of the electron-hole wave function overlap (Γ_{e-hh}) to 58.6% in the Increased-Al-composition graded QWs, as compared to the QW without grading ($\Gamma_{e-hh} = 40.4\%$) and reverse grading ($\Gamma_{e-hh} = 33.6\%$). Further investigations show that the grading profile of the Al composition in the QWs, including either linearly increases or decreases along the growth direction and the thickness of graded QWs, determine the polarization electrical field in the QWs and as a result, significantly affecting the performance of the devices. In the end, a careful optimization of the graded QWs is called. The proposed structure with such unique graded QWs provides us an effective solution to suppress the QCSE effect in the pursuit of high-performance DUV emitters.

Index Terms: DUV LED, polarization, grading QW, QCSE.

1. Introduction

In recent years, III-nitride based deep-ultraviolet light-emitting diodes (DUV LEDs) show a wide range of applications and prospects in the air/water purification, disinfection/sterilization, and biochemical sensing/treatment [1], [2]. However, AlGaN-based DUV LEDs still suffer from a series of challenges. Firstly, the performance of DUV LED is limited by low internal quantum efficiency (IQE) which is attributed to the high threading dislocation density (TDD) of AlGaN epilayers [3], [4]. Secondly, because of a higher electron mobility than that of holes' [5], [6] and the difficulty of p-type doping compared with the n-type, the hole density is much lower than the electron density in the QWs [7], leading to a relatively large leakage current and low radiative recombination, especially in the AlGaN based DUV LED with high Al composition (Al% > 50%) [8]. Lastly, due to the natural existence of spontaneous polarization and piezoelectric component caused by the strain between AlGaN
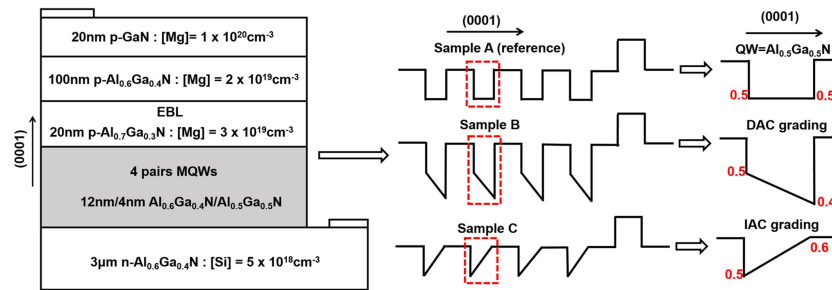
Fig. 1. The cross-sectional schematics and Al composition profiles of Sample A, B, and C with different Al-composition QW grading schemes.

epilayers with different Al composition, the strong quantum confined Stark effects (QCSE) in DUV LEDs separate the electron and holes within the QW and thus deteriorate the device performance [9].

To improve the IQE and eventually the performance of DUV LED, researchers have tentatively proposed various approaches. To reduce the TDD, several groups adopted patterned sapphire substrates (PSS) [10] or buffer-layer [11] or grew LEDs on native AlN substrates [12]. To achieve a uniform carrier distribution in the active region, Tsai *et al.* [13] employed the structure embedded with gradually increased quantum barriers (QBs) thicknesses from the n-side to p-side, generating a relative even distribution of the electrons and holes in the QWs. Arif *et al.* reported that InGaN QW with step-function-like improved the radiative recombination and optical gain, leading to the improvement of photoluminescence intensity and LED output power [14]. Furthermore, Zhang *et al.* [15] tried to enhance the hole injection by designing a p-EBL structure with graded Al composition. Alternatively, to suppress QCSE in the QWs, researchers grew the DUV LEDs along those nonpolar/semi-polar orientations [16] or introducing Si doping in the QBs to screen the internal polarization induced by electric field [17]. However, using the AlN substrates will increase the device fabrication cost tremendously, and the holes could be blocked if we doped QBs with Si-doping. Also, the mainstream of DUV LEDs is developed on the *c*-plane sapphire substrates rather on nonpolar/semi-polar substrates.

In this work, we propose a simple and unique multiple quantum well (MQW) architecture, in which the Al composition in the QW was graded from low to high along the growth direction. As a result, the interface charges at the QB/QW was reduced and the electrical field in QWs was also suppressed. Moreover, the bulk polarization-induced charges generated in the graded QW could create a reverse electrical field in the QWs thereby further screening the QCSE.

2. Structures and Parameters

The structures of DUV LEDs involved in this study are schematically shown in Fig. 1. These structures are composed of a 3-μm-thick n-type $Al_{0.6}Ga_{0.4}N$ layer (The Si doping concentration is 5 $\times 10^{18}$ cm^{-3} and the activation energy of Si is set to 15 meV [18]), followed by the active region which has five pairs of AlGaN/AlGaN MQWs, and then capped with the p-type region which consists of a 20-nm-thick p-$Al_{0.7}Ga_{0.3}N$ electron blocking layer (EBL) layer with a Mg doping concentration of 3 $\times$ 10^{19} cm^{-3}, a hole injection layer of 100-nm-thick p-$Al_{0.6}Ga_{0.4}N$ with Mg doping concentration of 2 $\times$ 10^{19} cm^{-3}, and finally a heavily doped p^{+}-GaN contact layer of 20-nm with Mg doping concentration of 1 $\times$ 10^{20} cm^{-3}. The Mg activation energy for the p-type $Al_{0.7}Ga_{0.3}N$, p-type $Al_{0.6}Ga_{0.4}N$, and p-type GaN are set to 520, 470 and 170 meV [19], respectively. In the active region, all three samples comprise four 4-nm-thick AlGaN QWs sandwiched by five 12-nm-thick $Al_{0.6}Ga_{0.4}N$ QBs. Sample A is designated as the reference structure which has flat QWs of $Al_{0.5}Ga_{0.5}N$. Sample B has a Decreased-Al-composition (DAC) linear-grading profile from 0.5 to 0.4 along the *c*-axis. On the contrary, Sample C has an Increased-Al-composition (IAC) linear-grading profile from 0.5 to 0.6.

We utilized a commercial software Advanced Physical Models of Semiconductor Devices (AP-SYS) provided by Crosslight, which can self-consistently solve drift-diffusion equations, Schrödinger and Poisson's equations with proper boundary conditions [20]. The Shockley-Read-Hall (SRH) recombination lifetime, Auger recombination coefficient and radiative recombination coefficient are
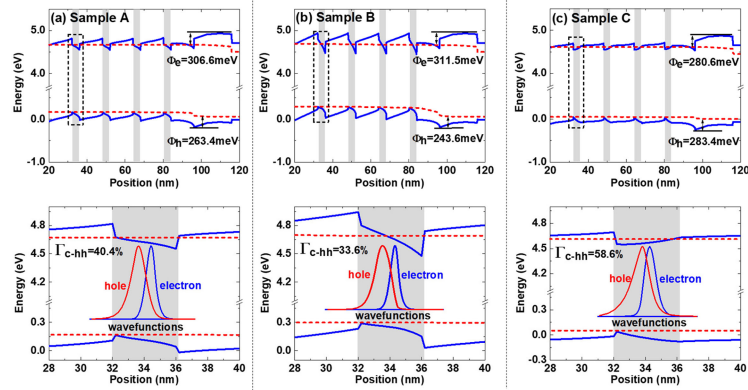
Fig. 2. Band diagrams for (a) Sample A, (b) Sample B, and (c) Sample C at 150 A/cm^2. Γ_{e-hh} represents the carrier wave function overlap. The effective barrier height of the p-EBL is also marked.

set to be 15 ns, 2.88×10^{-30} cm^6/s and 2.13×10^{11} cm^3/s, respectively [21], [22]. Furthermore, the band offset ratio of AlGaN alloy is set to 0.67/0.33 for the AlGaN/AlGaN QWs [23]. The interface charge densities are assumed to be 50% of total charges considering the screening effect of defects [24]. Considering polarization induced charges, we assumed a bulk charges density of -8.0×10^{18} cm^{-3} and $+8.9 \times 10^{18}$ cm^{-3} in Al$_{0.5 \rightarrow 0.4}$Ga$_{0.5 \rightarrow 0.6}$N/Al$_{0.6}$Ga$_{0.4}$N MQWs for Sample B and in Al$_{0.5 \rightarrow 0.6}$Ga$_{0.5 \rightarrow 0.4}$N/Al$_{0.6}$Ga$_{0.4}$N MQWs for Sample C [25]. The chip size is set to be 300 μm $\times$ 300 μm and some other band structure parameters including effective mass used in the simulation can be found elsewhere [26], [27]. The hole and electron mobility of AlGaN is based on previous reports and the alloy mobility model inside APSYS [18], [28].

3. Results and Discussions

The calculated band diagrams as well as the wave functions of electrons and holes for those three samples are plotted in Fig. 2(a)–(c). The blue line in Fig. 2(a) shows that the energy band edges of each QW for Sample A have significantly bent. We suspect that the electrons would strongly accumulate locally near p-side in the QW, while the holes accumulating near n-side in the QW. Such behavior of electrons and holes accumulating at different sides of QW becomes more problematic for Sample B. However, for Sample C, the conduction band of QW becomes flatter and both electrons and holes can be accumulated locally near the n-side in the QW, as a result of the linear change of the Al composition from 0.5 to 0.6 in QW along the c-axis [29]. Consequently, Sample C has the highest electron and hole wavefunction overlap value (Γ_{e-hh}) of 58.6%, comparing to Sample A and B which has only 40.4% and 33.6%. Regarding the effective conduction band potential barrier height in the p-EBL (Φ_e), Sample B with DAC grading QWs shows a higher value (311.5 meV) of Φ_e than that of both Sample A (306.6 meV) and Sample B (280.6 meV), which means that Sample B has the strongest electron blocking capability. For the effective valence band potential barrier height in p-EBL (Φ_h), Sample B shows the smallest value (243.6 meV) than the values of both Sample A (263.4 meV) and Sample B (283.4 meV), which suggests that Sample B has the highest hole injection efficiency.

As illustrated in Fig. 3(a), the smallest electric field intensity can be observed in the QWs of Sample C, leading to the biggest value of Γ_{e-hh}. This is attributed to the decreased density of piezoelectric polarization induced charge (ΔP^{pz}) caused by the compressive strain in the QWs. Besides, the discontinuity of spontaneous polarization in the interface of the QB/QW also contributes to the increase of spontaneous polarization induced charge density (ΔP^{sp}) [30]. The addition of these two types of polarization induced charge density can be expressed by the formula: $\Delta P^{tot} = \Delta P^{pz} + \Delta P^{sp}$. ΔP^{tot} represents the total polarization induced charge density that will directly affect the electric field strength in QW based on the formula: $E_w \approx l_b \cdot \Delta P^{tot}/(l_b \cdot \varepsilon_w + l_w \cdot \varepsilon_b)$ [31]. E_w is electric field in QWs, and l_b and l_w represent the width of QBs and QWs. Therefore, due to the suppressed ΔP^{sp} and ΔP^{pz}, the strength of the electric field decreased obviously in Sample C. Moreover, the positive bulk polarization charges in Sample C can also be generated owing to the reverse polarization-induced
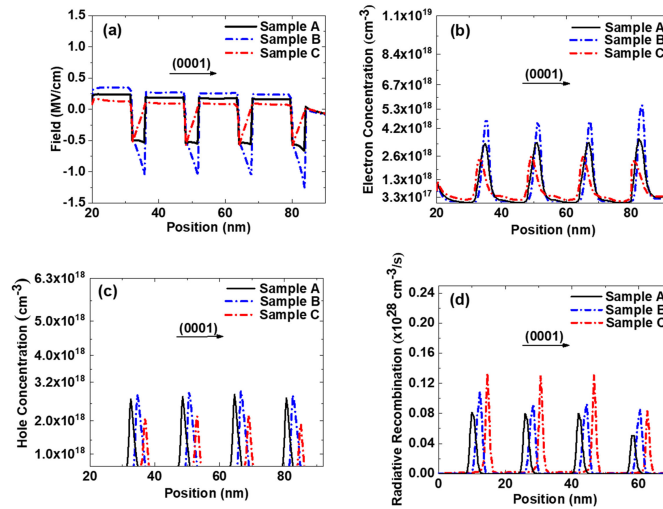
Fig. 3. (a) Electric field profile (b) Electron concentration profiles (c) Hole concentration profiles (d) Radiative recombination rate (R_{rad}) in the QWs of Sample A, B, and C at 150 A/cm^2. In order to present the curves more clearly, the relative position of the peaks was deliberately changed in fig. 3. (c) and (d).
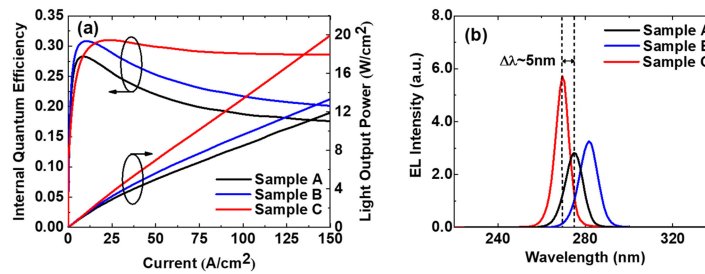

Fig. 4. (a) Light output power and IQE as a function of the injection current levels. (b) EL spectra for Sample A and Sample B at 150 A/cm^2.

electric field in the QW, further weakening the electric field. In other words, Sample C possesses the smallest electric field intensity in QBs, which can be explained by the equation, $E_b \cdot l_b = E_w \cdot l_w$ [31]. When E_w becomes smaller, the value of E_b decreases, leading to a flatter QB in Sample C, as shown in Fig. 2(c). Fig. 3(b) and (c) exhibit that the average electron and hole concentrations in the three samples, and we found it decreases from Sample B, Sample A to Sample C. Sample C has the smallest electron concentration due to the lowest value of Φ_e in the p-EBL. However, it seems that hole concentration in Sample C is relatively low which can be attributed to the highest value of Φ_h in the p-EBL. Nevertheless, Sample C still presents the largest value of average radiative recombination according to Fig. 3(d) because it has the largest value of Γ_{e-hh}.

Moreover, the light output power (LOP) and IQE as a function of injection currents for Sample A, B and C are also investigated, as shown in Fig. 4(a). Sample C has much greater LOP, a 67.04% higher than that of the reference structure (Sample A) because of the enhanced value of Γ_{e-hh}. It suggests that even though the structure of IAC grading QW would slightly reduce the carrier concentration in the active region, it can greatly improve the overlap of wave function and thus still enhance the performance of LED. However, Sample B has the highest electron and hole concentration inside the active region (as shown in Fig. 3(b) and (c)), but its output power did not reach as high as the Sample C. The reason behind is that the Γ_{e-hh} of the Sample B is even lower than the reference structure because it has very large electrical field inside QWs. Furthermore, Sample C has the smallest efficiency droop value of only 7.59%, as compared with Sample A and C that have efficiency droop of 39.34% and 35.76%, respectively. Fig. 4(b) shows the EL spectra for the three samples. Sample C has a higher EL intensity than that of Sample A by 74.78%, and Sample B exhibits relatively poor EL behavior and only has a slightly higher EL intensity by 16.18%
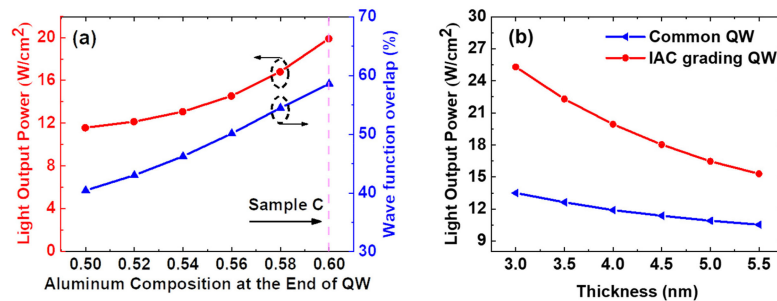
Fig. 5. (a) LOP and Γ_{e-hh} as a function of the Al composition at the end of QW (b) The LOP as a function of QW thickness.

compared with Sample A. Meanwhile, the peak emission wavelength of Sample C shows a blue shift of ~5 nm while Sample B has a slight red shift of 6 nm, as a result of compositional grading in QWs in which the effective bandgap was enlarged/shrunk decrease correspondingly.

To further optimize the IAC grading structure, we also calculated the evolution of LOP and Γ_{e-hh} when the Al-composition at the end of the QWs increases from 0.5 to 0.6 while maintaining the same value of beginning Al-composition (0.5) in the QWs. As shown in Fig. 5(a), the value of LOP increases with the ending Al-composition increasing from 0.5 to 0.6 because of the rapid increase of the Γ_{e-hh}. Therefore, considering the balance between carrier concentration and Γ_{e-hh}, we got the best structure with the highest LOP value when the Al-composition of each QW increased from 0.5 to 0.6 linearly. A balance between the carrier concentration and Γ_{e-hh} should be taken into consideration to maximize the LOP and minimize the IQE droop of such LEDs incorporated with graded QW structure.

In Fig. 5(b), based on the previous results, we varied the QW width of both reference structure with flat QWs and optimized structure with IAC grading QWs (grading from 0.5 to 0.6). It indicates that the value of LOP increases with decreasing QW thickness and finally the LOP value of the optimized LED with 3 nm-IAC grading QWs is more than twice higher than that of the reference sample. It is because that the values of Γ_{e-hh} in the QWs increase as the thickness of the QW decreased since the QCSE in the QWs becomes weaker [32]. It is worth noting that the LED with IAC grading QW still shows relatively better performance than reference Sample when the QW thickness increases from 3 nm to 5.5 nm, which is critical for fabricating high brightness AlGaN-based DUV LED. Although this is a theoretical work focusing on the QCSE suppression via graded AlGaN QWs to enhance the DUV LED performance, we expect that it is straightforward to realize such structures via conventional metal organic chemical vapor deposition (MOCVD) [33], [34] and molecular beam epitaxy (MBE) [35]–[37] by precisely controlling the Al/III molar ratio in monolayer-scale during the epitaxial process.

4. Conclusion

In this work, we numerically investigated a unique design of an AlGaN QW with grading Al-composition and its impact on the tunability of the polarization field and the carrier wave-function overlap, the radiative recombination rate and the optical output power of DUV LEDs. Simulation results indicated that the DUV LED with the IAC grading has the best optical performance attributing to IAC grading effectively screen the QCSE in the QWs, leading to a large wave function overlap of 58.6%. Though the carrier concentration in the QWs has slightly decreased, the DUV LED with IAC grading QWs still has the obvious enhancement of the IQE and LOP. Furthermore, we found that IAC grading from 0.6 to 0.5 shows the best performance. This approach provides a new feasible scheme for the future development of efficient DUV LEDs.

References

[1] T. D. Moustakas and R. Paiella, "Optoelectronic device physics and technology of nitride semiconductors from the UV to the terahertz," *Rep. Prog. Phys.*, vol. 80, no. 10, 2017, Art. no. 106501.
[2] Z.-H. Zhang *et al.*, "Hole transport manipulation to improve the hole injection for deep ultraviolet light-emitting diodes," *ACS Photon.*, vol. 4, no. 7, pp. 1846–1850, 2017.

[3] M. Kneissl and J. Rass, *III-Nitride Ultraviolet Emitters*. Berlin, Germany: Springer, 2016, ch. 5, pp. 115–136.
[4] T. D. Moustakas, "Ultraviolet optoelectronic devices based on AlGaN alloys grown by molecular beam epitaxy," *MRS Commun.*, vol. 6, no. 3, pp. 247–269, 2016.
[5] X. Hai, R. T. Rashid, S. M. Sadaf, Z. Mi, and S. Zhao, "Effect of low hole mobility on the efficiency droop of AlGaN nanowire deep ultraviolet light emitting diodes," *Appl. Phys. Lett.*, vol. 114, no. 10, 2019, Art. no. 101104.
[6] V. O. Turin, "A modified transferred-electron high-field mobility model for GaN devices simulation," *Solid-State Electron.*, vol. 49, no. 10, pp. 1678–1682, 2005.
[7] S. Selberherr, *Analysis and Simulation of Semiconductor Devices*. New York, NY, USA: Springer, 1984.
[8] H. Sun *et al.*, "Graded-Index separate confinement heterostructure AlGaN nanowires: Toward ultraviolet laser diodes implementation," *ACS Photon.*, vol. 5, no. 8, pp. 3305–3314, 2018.
[9] F. Wu *et al.*, "Significant internal quantum efficiency enhancement of GaN/AlGaN multiple quantum wells emitting at ∼350 nm via step quantum well structure design," *J. Phys. D—Appl. Phys.*, vol. 50, no. 24, 2017, Art. no. 245101.
[10] P. Dong *et al.*, "282-nm AlGaN-based deep ultraviolet light-emitting diodes with improved performance on nano-patterned sapphire substrates," *Appl. Phys. Lett.*, vol. 102, no. 24, 2013, Art. no. 241113.
[11] K. Ban *et al.*, "Internal quantum efficiency of whole-composition-range AlGaN multiquantum wells," *Appl. Phys. Exp.*, vol. 4, no. 5, 2011, Art. no. 052101.
[12] Z. Bryan, I. Bryan, J. Xie, S. Mita, Z. Sitar, and R. Collazo, "High internal quantum efficiency in AlGaN multiple quantum wells grown on bulk AlN substrates," *Appl. Phys. Lett.*, vol. 106, no. 14, 2015, Art. no. 142107.
[13] M.–C. Tsai, S.-H. Yen, and Y.-K. Kuo, "Deep-ultraviolet light-emitting diodes with gradually increased thicknesses from n-layers to p-layers," *Appl. Phys. Lett.*, vol. 98, no.11, 2011, Art. no. 111114.
[14] R. A. Arif, Y-K. Ee, and N. Tansu, "Polarization engineering via staggered InGaN quantum wells for radiative efficiency enhancement of light emitting diodes," *Appl. Phys. Lett.*, vol. 91, no. 9, 2007, Art. no. 091110.
[15] Z.–H. Zhang *et al.*, "Increasing the hole energy by grading the alloy composition of the p-type electron blocking layer for very high-performance deep ultraviolet light-emitting diodes," *Photon. Res.*, vol. 4, pp. B1–B6, 2019.
[16] J. Bruckbauer *et al.*, "Spatially-resolved optical and structural properties of semi-polar Al$_x$Ga$_{1-x}$N with *x* up to 0.56," *Sci. Rep.*, vol. 7, 2017, Art. no. 10804.
[17] K. Tian *et al.*, "Investigations on AlGaN-based deep ultraviolet light-emitting diodes with si doped quantum barriers of different doping concentrations," *Phys. Status Solidi-Rapid Res. Lett.*, vol. 12, no. 1, 2018, Art. no. 1700346.
[18] R. Collazo *et al.*, "Progress on n-type doping of AlGaN alloys on AlN single crystal substrates for UV optoelectronic applications," *Phys. Status Solidi C*, vol. 8, no. 7/8, pp. 2031–2033, 2011.
[19] K. B. Nam, M. L. Nakarmi, J. Li, J. Y. Lin, and H. X. Jiang, "Mg acceptor in AlN probed by deep ultraviolet photolumi-nescence," *Appl. Phys. Lett.*, vol. 83, no. 5, pp. 878–880, 2003.
[20] [Online]. Available: http://www.crosslight.com/. Accessed on: Mar. 2019.
[21] J. Yun, J. Shim, and H. Hirayama, "Analysis of efficiency droop in 280 nm AlGaN multiple-quantum-well light-emitting diodes based on carrier rate equation," *Appl. Phys. Exp.*, vol. 8, no. 2, 2015, Art. no. 022104.
[22] Z. Ren *et al.*, "III-nitride deep UV LED without electron blocking layer," *IEEE Photon. J.*, vol. 11, no. 2, 2019, Art. no. 8200511.
[23] C. Coughlan, S. Schulz, M. A. Caro, and E. P. Reilly, "Band gap bowing and optical polarization switching in Al$_{1-x}$Ga$_x$N alloys," *Phys. Status Solidi B-Basic Solid State Phys.*, vol. 252, no. 5, pp. 879–884, 2015.
[24] Y.-K. Kuo, J.-Y. Chang, F.-M. Chen, Y.-H. Shih, and H.-T. Chang, "Numerical investigation on the carrier transport characteristics of AlGaN deep-UV Light-emitting diodes," *IEEE J. Quantum Electron*, vol. 52, no. 4, Apr. 2016, Art. no. 3300105.
[25] V. Fiorentini, F. Bernardini, and O. Ambacher, "Evidence for nonlinear macroscopic polarization in III-V nitride alloy heterostructures," *Appl. Phys. Lett.*, vol. 80, no. 7, pp. 1204–1206, 2002.
[26] S. M. Zse. *Physics of Semiconductor Devices*, 2nd ed. New York, NY, USA: Wiley, 1981.
[27] J.-Y. Chang, B.-T. Liou, M.-F. Huang, Y.-H. Shih, F.-M. Chen, and Y.-K. Kuo, "High-efficiency deep-ultraviolet light-emitting diodes with efficient carrier confinement and high light extraction," *IEEE Trans. Electron Devices*, vol. 66, no. 2. pp. 976–982, Feb. 2019.
[28] M. L. Nakarmi, K. H. Kim, M. Khizar, Z. Y. Fan, J. Y. Lin, and H. X. Jiang, "Electrical and optical properties of Mg-doped Al$_{0.7}$Ga$_{0.3}$N alloys," *Appl. Phys. Lett.*, vol. 86, 2005, Art. no. 092108.
[29] Z.-H. Zhang *et al.*, "InGaN/GaN multiple-quantum-well light-emitting diodes with a grading InN composition suppressing the Auger recombination," *Appl. Phys. Lett.*, vol. 105, no. 3, 2014, Art. no. 033506.
[30] O. Ambacher *et al.*, "Two-dimensional electron gases induced by spontaneous and piezoelectric polarization charges in N- and Ga-face AlGaN/GaN heterostructures," *J. Appl. Phys.*, vol. 85, pp. 3222–3223, 1999.
[31] Z. Zhang, W. Liu, Z. Ju, S. Tan, Y. Ji, and H. Demir, "Self-screening of the quantum confined Stark effect by thepolar-ization induced bulk charges in the quantum barriers," *Appl. Phys. Lett.*, vol. 104, no. 24, 2014, Art. no. 243501.
[32] A. T. M. G. Sarwar, B. J. May, and R. C. Myers, "Effect of quantum well shape and width on deep ultraviolet emission in AlGaN nanowire LEDs," *Phys. Status Solidi A—Appl. Mater. Sci.*, vol. 213, no. 4, pp. 947–952, 2016.
[33] C. R. Haughn *et al.*, "Highly radiative nature of ultra-thin c-plane Al-rich AlGaN/AlN quantum wells for deep ultraviolet emitters," *Appl. Phys. Lett.*, vol. 114, no. 10, 2019, Art. no. 102101.
[34] W. Guo *et al.*, "Lateral-Polarity structure of AlGaN quantum wells: A promising approach to enhancing the ultraviolet luminescence," *Adv. Funct. Mater.*, vol. 28, no. 32, 2018, Art. no. 1802395.
[35] S. M. Islam *et al.*, "MBE-grown 232–270nm deep-UV LEDs using monolayer thin binary GaN/AlN quantum heterostruc-tures," *Appl. Phys. Lett.*, vol. 110, no. 4, 2017, Art. no. 041108.
[36] P. Mishra *et al.*, "On the optical and microstrain analysis of graded InGaN/GaN MQWs based on plasma assisted molecular beam epitaxy," *Opt. Mater. Exp.*, vol. 6, no. 6, pp. 2052–5062, 2016.
[37] H. Sun, J. Yin, E. Pecora, L. Dal Negro, R. Paiella, and T. D. Moustakas, "Deep-ultraviolet emitting AlGaN multiple quantum well graded-index separate-confinement heterostructures grown by MBE on SiC substrates," *IEEE Photon. J.*, vol. 9, no. 4, 2017, Art. no. 2201109.